JOURNAL OF MATERIALS SCIENCE 33 (1998) 995–1001

Long-term thermal stability and mechanical properties of aluminium titanate at 1000–1200°C

T.S. LIU, D.S. PERERA
Australian Nuclear Science and Technology Organisation (ANSTO), Menai, NSW 2234, Australia
E-mail:clsp@ansto.gov.au

Two aluminium titanate (AT) ceramics containing magnesium and iron were sintered to study their high-temperature mechanical property and thermal stability. Both materials exhibited a pronounced inelastic stress–strain behaviour which is caused by extensive microcracks. The microcracking also led to an increasing *R*-curve behaviour which was measured in the Mg–AT material in the as-sintered state. At 1000 °C, crack healing took place which led to an increase in the strength and Young's modulus. At 1100 °C, the glassy phase started to soften which resulted in a reduction of the strength and Young's modulus. Thermal stability was assessed after annealing at 1000, 1100 and 1200 °C for 250 and 1000 h in air. Although the Fe–AT material did not show any significant decomposition and degradation in mechanical properties, the Mg–AT material annealed at 1000 and 1100 °C showed pronounced decomposition into corundum and rutile. The decomposition led to a brittle fracture, but increased the strength and Young's modulus. Both materials showed a lower coefficient of thermal expansion ($< 0.2 \times 10^{-6} K^{-1}$) than that of stoichiometric aluminium titanate. The results are discussed with respect to the microstructure and phase relationship. © *1998 Chapman & Hall*

1. Introduction

Aluminium titanate, Al_2TiO_5(AT), is formed by a solid-state reaction of equimolar mixtures of Al_2O_3 and TiO_2 above 1280 °C [1]. It has a low bulk thermal expansion because of extensive microcracking which results from the highly anisotropic coefficient of thermal expansion (CTE) of its crystallographic axes. AT dissociates to corundum and rutile in the temperature range 750–1280 °C, and to overcome this dissociation, stabilizers such as Fe_2O_3, MgO or SiO_2 are added [2]. The first two oxides form pseudobrookite structures Fe_2TiO_5 and $MgTi_2O_5$ with TiO_2, respectively. The Fe_2TiO_5 and $MgTi_2O_5$ form complete solid solutions with AT. The SiO_2, however, forms only a limited solid solution [3]. Day and Locker [4] found no dissociation of AT with 20 mol % additions of Fe_2TiO_5 at 1000 and 1200 °C up to 1000 h, but with the same amount of $MgTi_2O_5$ for the same time there was complete dissociation at 1000 °C and partial dissociation at 1200 °C. One disadvantage of these additions is that they could increase the bulk CTE of AT because the bulk CTE of the Fe_2TiO_5 and $MgTi_2O_5$ is much higher than that of AT [5, 6].

For refractory applications, long-term thermal stability and mechanical properties are important if these materials are to be used between 1000 and 1200 °C. In this work, two modified AT materials with MgO and Fe_2O_3 as stabilizer, were produced to investigate their mechanical properties and long-term thermal stability and degradation in mechanical properties. The mechanical properties were measured at 25, 1000, 1100 and 1200 °C for the as-sintered materials, and at 25 °C for materials annealed for 250 h at 1000, 1100 and 1200 °C. Long-term thermal stability was studied by annealing the materials for 1000 h at 1000 and 1200 °C. The mechanical properties and thermal stability of the materials are correlated to the microstructure and phase compositions.

2. Experimental procedure

Two batches of materials (> 20 kg) were produced to obtain the expected phases listed in Table I. The compositions were made from alumina (AMS9-Sumitomo Chemicals, Japan), rutile (Tiona RCL 181-SCM Chemicals, Australia), magnesia (Univar, Sigma Chemicals), iron oxide (Sigma) and silica (Silica Fume X50-Degusa, Germany) by high-speed mixing for 1 h in water with 1% poly vinyl alcohol added as a binder. The slurry was spray-dried to produce an agglomerate-free powder. From the powders, cylindrical and rectangular shapes, which weighed about 1 kg each, were formed by cold isostatic pressing in polymer moulds at 200 MPa pressure. After binder burn out at 800 °C for 4 h, the blocks were sintered in air at 1400 °C for 6 h at 1 K min^{-1} heating and cooling rates.

The as-sintered and annealed specimens were cut and mounted in resin and polished to 1 μm finish. They were examined by scanning electron microscopy (SEM) and analysed by energy dispersive X-ray

spectroscopy (EDS). Portions of specimens were ground to $<75\ \mu m$ and analysed by X-ray diffraction analysis (XRD) with CoK_α radiation. The density and porosity of the bars were determined according to AS 1774.5 [7], but only the apparent solid density values are reported. From the same two materials, specimens $6\ mm \times 6\ mm \times 10\ mm$ were heated at $5\ K\ min^{-1}$ in a dilatometer in air from 25°–1250 °C to measure their CTE.

Specimens of size $3.5\ mm \times 4.5\ mm \times 50\ mm$ and $3.5\ mm \times 6\ mm \times 50\ mm$ were cut from blocks for mechanical testing. Four-point bend tests were conducted on ground bars at 25, 1000, 1100 and 1200 °C with inner and outer span widths of 20 and 40 mm, respectively. Six samples were used to measure the strength and stress–strain curves. The tests were conducted in position control with a rate of $0.001\ mm\ s^{-1}$, where six samples were tested at each temperature. For materials with pronounced inelastic behaviour, the true stress, σ, on the tensile surface of a four-point-bending specimen is different from the elastic stress due to the inelastic deformation. Therefore, the true stress is calculated from Equation 1 [8]

$$\sigma = \frac{(L_0 - L_i)}{wh^2}\left(P + \frac{\delta}{2}\frac{\partial P}{\partial \delta}\right) \quad (1)$$

where L_0 and L_i are the outer and inner span width of the four-point-bending jig, respectively, w is the specimen width, h the specimen height, P the load, δ the beam deflection measured by a linear variable displacement transducer (LVDT), and $\partial P/\partial\delta$ is the differential of the P–δ curve. The brittleness function χ can be calculated from Equation 2 [9]

$$\chi = \frac{U_e}{U_T} = \frac{\sigma_f^2}{2E\int_0^{\varepsilon_f}\sigma\, d\varepsilon} \quad (2)$$

where U_e is the elastic stored energy (assuming linear elastic behaviour), U_T the actual energy absorbed in deformation of a certain strain ε_f, σ the stress, ε the strain, σ_f the strength, and E the Young's modulus. For ideal linear-elastic materials $\chi = 1$, whereas the lower the χ, the more pronounced is the inelastic behaviour of a material.

Crack resistance (R-curve) was measured on Mg–AT at room temperature in compact tension (CT) tests. The detailed experimental procedure was described previously [10]. Four-point bending specimens of the same size as above were annealed in a furnace in air at 1000 and 1200 °C for 200, 250 and 1000 h and at 1100 °C for 250 h at $5\ K\ min^{-1}$ heating and cooling rates. Four-point bending tests were conducted on the annealed specimens at room temperature to measure the mechanical properties after annealing.

TABLE I Aluminium titanate batches prepared

Materials	Phases expected
Fe–AT	95% (solid solution of Al_2TiO_5 and Fe_2TiO_5, of composition $Al_{1.57}Fe_{0.43}TiO_5$), 2% corundum, 3% glass.
Mg–AT	97% (solid solution of Al_2TiO_5 and $MgTi_2O_5$, of composition $Al_{1.62}Mg_{0.19}Ti_{1.19}O_5$), 3% glass.

3. Results and discussion

3.1. Material characterization

The apparent solid density values and the XRD analysis of the materials before and after annealing are listed in Table II. In the as-sintered state, the apparent solid density of Fe–AT is higher than the Mg–AT. For both AT materials, the XRD analysis showed an enlarged unit-cell of AT as major phase, while the Fe–AT contained a minor amount of corundum. Phase analysis after high-temperature annealing is described in Section 3.2.

Because of the complete solid solution between AT and Fe_2TiO_5 and between AT and $MgTi_2O_5$, it was possible to calculate the compositions of the AT phases in Fe–AT and Mg–AT materials from the linear variation of lattice parameters between these phases. From the XRD measurements, lattice

TABLE II The density and XRD analysis of the materials after annealing. *Note*: For 200 h both materials at the two temperatures showed complete stability

Materials	Annealing conditions		App. solid density, ($g\ cm^{-3}$)	XRD analysis[a]
	(°C)	(h)		
Fe–AT	As-sintered		3.78	AT*, C
	1000	250	3.75	AT*, C
	1000	1000	3.75	AT*, C
	1200	250	–	AT*, C
	1200	1000	3.74	AT*, C
Mg–AT	As-sintered		3.60	AT*
	1000	250	3.87	AT (vw), C (s), R (s), sp (w)
	1000	1000	–	C (s), R (s), sp (w)
	1100	250	3.89	C (s), R (s), sp (w)
	1200	250	3.65	AT (vs), C (w), R (w), sp (w)
	1200	1000	–	AT (m), C (m), R (s), sp (w)

[a] AT = aluminium titanate unit-cell almost equals stoichiometric AT, AT* = enlarged unit-cell compared to AT, C = corundum, R = rutile, sp = $MgAl_2O_4$ spinel, v = very, s = strong, m = medium, w = weak.

TABLE III Compositions and theoretical densities of aluminium titanates

Materials	Composition of solid-solution phases		Theoretical density ($g\,cm^{-3}$)[a]
	From starting compositions	By unit-cell measurements	
Fe–AT	$Al_{1.57}Fe_{0.43}TiO_5$	$Al_{1.65}Fe_{0.35}TiO_5$	3.83
Mg–AT	$Al_{1.62}Mg_{0.19}Ti_{1.19}O_5$	$Al_{1.74}Mg_{0.13}Ti_{1.13}O_5$	3.70
Al_2TiO_5	–	–	3.70
Fe_2TiO_5	–	–	4.35
$MgTi_2O_5$	–	–	3.65

[a] Assumed to be equal to X-ray density.

parameters of the "AT phases" were calculated from which the compositions were calculated using the X-ray data from Bayer [11]. The theoretical density was calculated from the X-ray density using the unit-cell volumes [12] and the values are listed in Table III along with the compositions. The compositions determined from the lattice parameters are slightly less-rich in iron and magnesium compared to the starting compositions. This implies either volatilization of these elements or their presence in the glassy phase. The latter is shown to be the case below.

The scanning electron micrographs of the as-sintered materials are shown in Fig. 1. Extensive microcracking can be observed for both types of AT materials. The grain size of Mg–AT is larger than that of Fe–AT for the as-sintered materials, where particle pinning by the corundum may prevent grain growth. The EDS analysis of the white contrast phase shown in Fig. 1a revealed aluminium, titanium and iron, (i.e. iron aluminium titanate) and the dark-grey phase aluminium (i.e. corundum). The black contrast regions are either porosity or the mounting resin. The black contrast region marked with an arrow (Fig. 1a) showed weak EDS peaks of Si, Al and Fe, which probably is a glassy region. The lighter contrast phase shown in Fig. 1b gave EDS peaks for aluminium, titanium and magnesium (i.e. magnesium aluminium titanate) and the region marked with an arrow showed the presence of silicon, aluminium and magnesium. The latter region is probably a glassy phase. The black contrast areas are porosity or the mounting resin. The first liquid-phase formation in the $MgO–Al_2O_3–SiO_2$ system is at 1355 °C [13], hence the presence of a glassy phase would be expected in Mg–AT after sintering at 1400 °C. The $Al_2O_3–SiO_2–TiO_2$ system has a eutectic at 1480 °C [14] and in the presence of Fe_2O_3 and with the minor impurities present in the raw materials it is possible to form a liquid phase at 1400 °C, explaining the presence of a small region of glass (Fig. 1a). The presence of more liquid phase in the Mg–AT will promote the coarsening of AT grains by Ostwald ripening, as shown previously for a similar system [12].

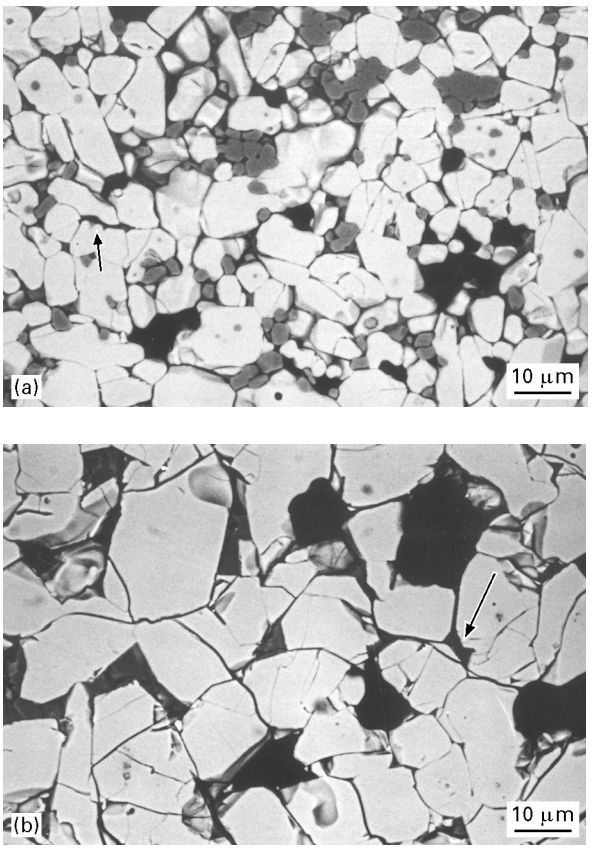

Figure 1 Microstructure of (a) the Fe–AT and (b) Mg–AT in the as-sintered state.

3.2. Long-term thermal stability

Fig. 2 shows the microstructure of the Fe–and Mg–AT under the SEM after long-term annealing at elevated temperatures. The microstructure of the Fe–AT is almost unchanged after annealing at 1000, 1100 and 1200 °C, which indicates that there are no dissociation products in Fe–AT as observed previously [4]. The Mg–AT annealed at 1000 and 1100 °C for 250 and 1000 h showed a distinct change in microstructure. The EDS analysis indicates that the dark grains are rich in aluminium (i.e. corundum) and the light phase is rich in titanium (i.e. rutile). The SEM micrographs of Mg–AT annealed at 1000 and 1100 °C for 250 h showed very little microcracking and smaller grain size of the dissociation products. In some areas, spinel phase was also observed under the SEM. The dissociation of Mg–AT is more pronounced at 1000 °C than at 1200 °C, in agreement with Day and Locker [4]. These results agree with the XRD analysis (Table II) for the 1200 °C/1000 h annealed Mg–AT material. The apparent solid density values also agree with the XRD analysis, where there is an increase in density when dissociation products such as corundum (density =

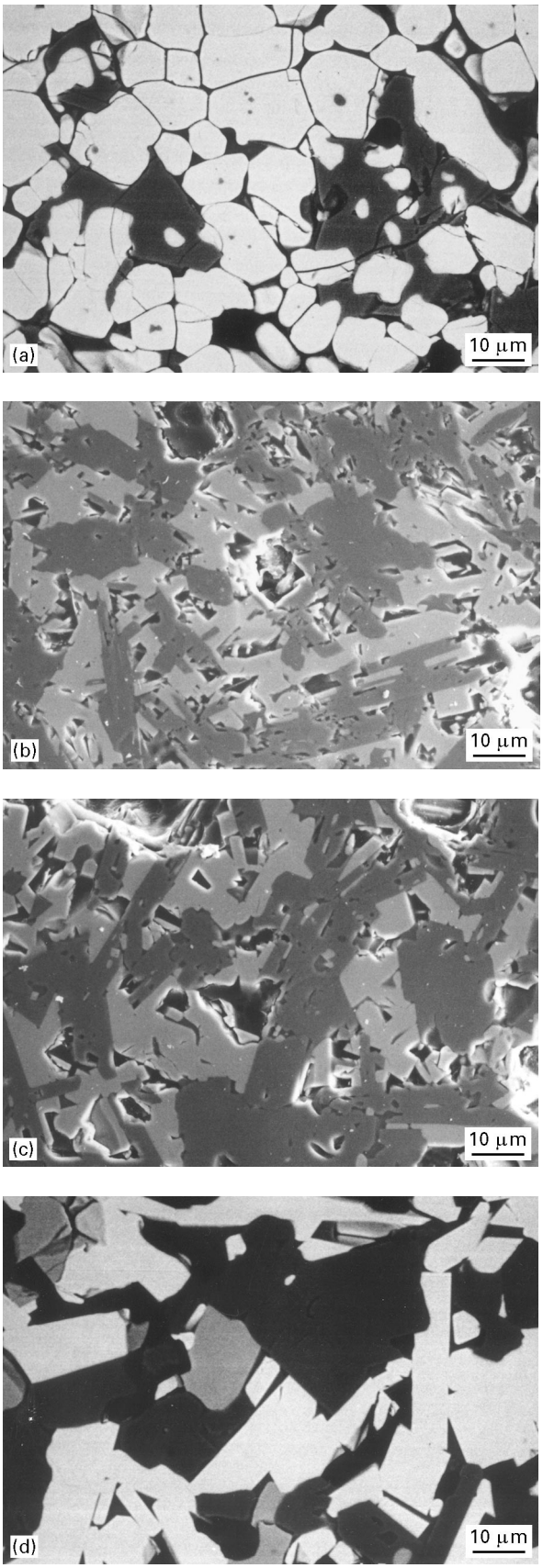

Figure 2 Microstructure of the Fe–AT and Mg–AT after high-temperature annealing. (a) Fe–AT annealed at 1200 °C for 1000 h; (b) Mg–AT annealed at 1000 °C for 250 h; (c) Mg–AT annealed at 1100 °C for 250 h; (d) Mg–AT annealed at 1200 °C for 1000 h.

3.99 g cm^{-3}) and rutile (density = 4.26 g cm^{-3}) are present. After annealing, the corundum phase has coarsened much more than the titanate phase (Figs 1 and 2).

The instability of AT is not yet clearly understood, in spite of several published works referred to elsewhere [2]. Some insight could be gained by studying the structure of the pseudobrookites. The AlO_6 octahedron in AT is distorted as it shows a tendency for tetrahedral coordination [11]. Tilloca [15] suggested that the Al^{3+} (ionic radius = 0.053 nm) is slightly too small for the octahedral site, whereas, Fe^{3+} (ionic radius = 0.064 nm) and Mg^{2+} (ionic radius = 0.078 nm) fit in well. The similarity of the Fe^{3+} cation size to Ti^{4+} (ionic radius = 0.068 nm) involves a higher thermal stability because the octahedra are much less distorted than that of AT or to a lesser extent than that of $MgTi_2O_5$. Ishitsuka *et al.* [3] found that it was possible to replace Ti^{4+} by Si^{4+} to a limited extent in the AT structure which resulted in thermal stability. In this work, also, it may occur with the SiO_2 added, but it is difficult to prove it. Ishitzuka *et al.* investigated their stability for only about 200 h, for at that time even the Mg–AT is quite stable both at 1000 and 1200 °C.

3.3. Short-term mechanical properties

Fig. 3 shows stress–strain curves of the two AT materials in the as-sintered state as a function of the testing temperature. Both compositions showed distinct non-linear, inelastic stress–strain curves, which is attributed mainly to widespread microcracking

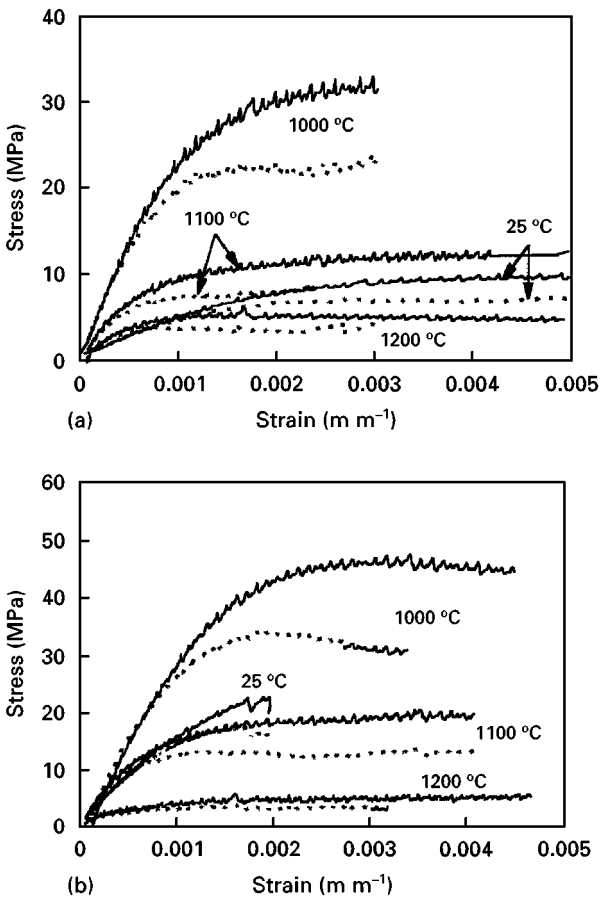

Figure 3 Stress–strain curves of (a) the Fe–AT and (b) Mg–AT in the as-sintered state as a function of the testing temperature. (∿∿) Elastic stress, (•••) true stress.

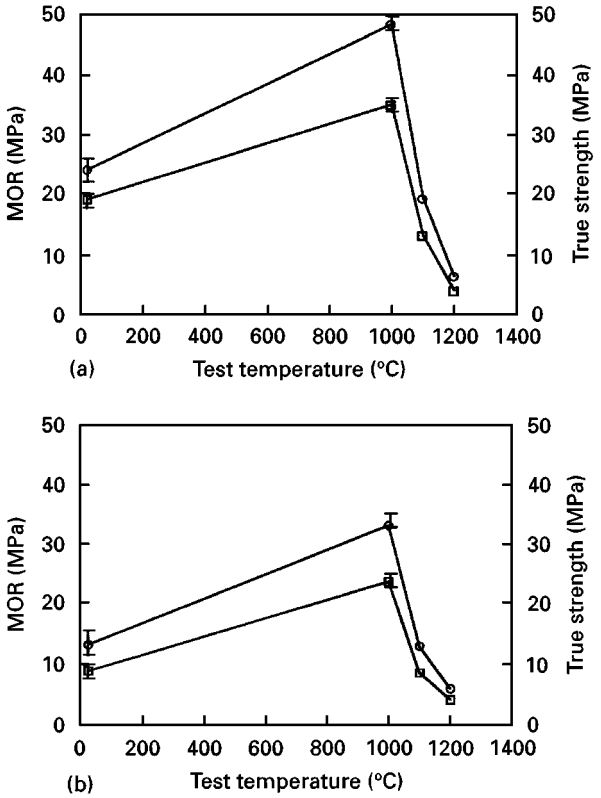

Figure 4 (○) MOR and (□) true strength of (a) the Fe–AT and (b) Mg–AT in the as-sintered state as a function of the testing temperature.

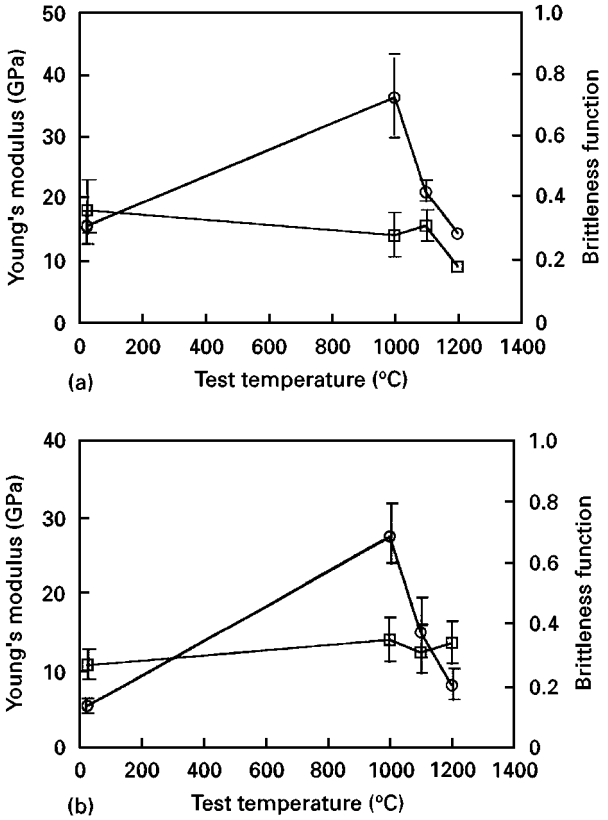

Figure 5 (○) Young's modulus and (□) brittleness function of (a) the Fe–AT and (b) Mg–AT in the as-sintered state as a function of the testing temperature.

(Fig. 1). From such curves, the modulus of rupture (MOR), true strength, Young's modulus, E, and brittleness function (χ) can be determined, which are shown in Figs 4 and 5. Both materials showed an increase in MOR, true strength and Young's modulus at 1000 °C. As observed in thermal cycling tests in the dilatometer [16], crack healing takes place at elevated temperature. Therefore, a higher strength and Young's modulus can be expected at these temperatures. At 1100 and 1200 °C, softening of the glassy phase occurred and dictates the mechanical behaviour, leading to a reduction in the strength and Young's modulus. The Fe–AT material showed slightly higher strength and Young's modulus than the Mg–AT material due to the smaller grain size resulting in less microcracking and due to the presence of corundum, as reported previously [17].

The brittleness function of the two AT materials is very low due to the extensive microcracking, as shown in Fig. 1. With increasing temperature the brittleness function increases slightly for the Mg–AT and decreases slightly for the Fe–AT. Fig. 6 shows R-curves of the Mg–AT measured in the CT tests. The crack resistance is increased with crack extension. A microstructure study on the side surface of the CT-specimens identified microcracking as the major toughening mechanism in the Mg–AT. Both the very low brittleness function and the increasing R-curve behaviour indicate a very high crack stability and thermal shock resistance. In fact, crucibles made from the Mg–ATs survived 15 air-quenches from 1500 °C, or 30 water quenches from 1000 °C [18]. The average

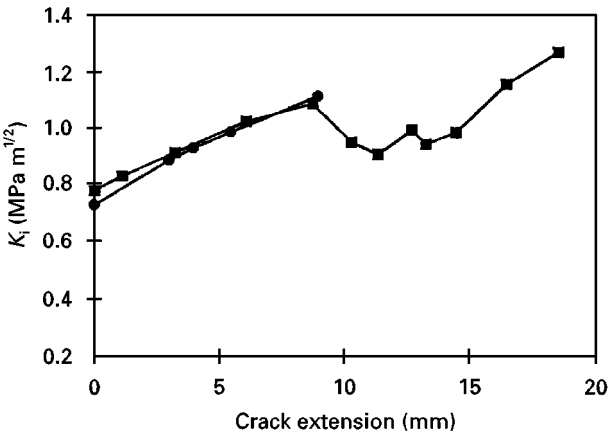

Figure 6 Crack resistance (R-) curve of the Mg–AT material measured in the CT tests at room temperature. (■) Sample 1, (●) sample 2.

coefficient of thermal expansion (CTE) is $<0.1 \times 10^{-6}$ K^{-1} between 20° and 1000 °C for both materials. The very high thermal shock resistance is caused by the very low CTE and high crack stability.

3.4. Long-term thermal degradation in mechanical properties

Fig. 7 shows the room-temperature stress–strain curves of the two AT materials after 250 h annealing at 1000, 1100 and 1200 °C. For the Fe–AT specimens inelastic stress–strain curves were observed after annealing at all temperatures, which are similar to

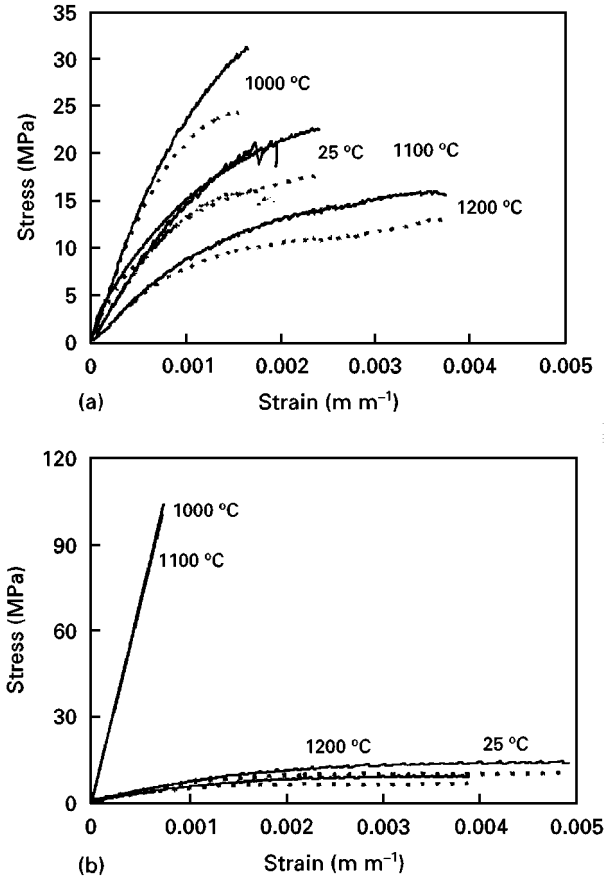

Figure 7 Stress–strain curves of (a) the Fe–AT and (b) Mg–AT measured at room temperature as a function of the annealing temperature. (—) Elastic stress, (▪ ▪ ▪) true stress.

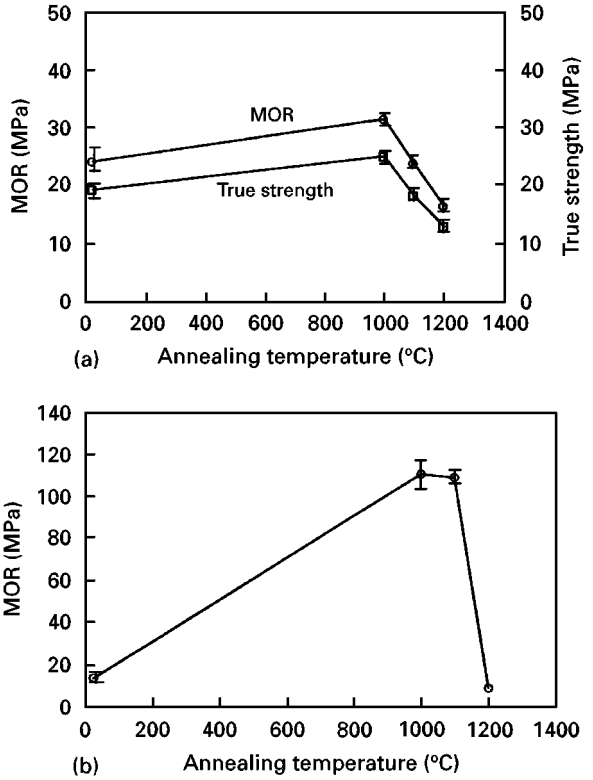

Figure 8 (○) MOR and (□) true strength of (a) the Fe–AT and (b) Mg–AT measured at room temperature as a function of the annealing temperature.

that measured in the as-sintered state. For the 1200 °C annealed Mg–AT specimens, an inelastic stress–strain curve was observed, which is similar to the stress–strain curve in the as-sintered state, while the specimens annealed at 1000 and 1100 °C exhibit a totally linear-elastic stress–strain curve. Figs 8 and 9 represent the room-temperature mechanical properties as a function of the annealing temperature. For the Mg–AT, a marked increase in strength, Young's modulus and brittleness function were observed after annealing at 1000 and 1100 °C. However, the 1200 °C annealed specimens showed similar mechanical properties to those in the as-sintered state. For the Fe–AT, the strength and Young's modulus showed a slight increase after annealing at 1000 and 1100 °C, followed by a slight decrease after annealing at 1200 °C. The brittleness function remained nearly unchanged after annealing. The mechanical properties agree with the microstructure and XRD results as discussed above, where Fe–AT is unchanged while Mg–AT is dissociated partially after 250 h annealing.

4. Conclusions

Two materials, one an iron aluminium titanate with minor phases of corundum and glass, and the other a magnesium aluminium titanate with a minor glassy phase were investigated for their thermal stability and mechanical properties. The results are summarized below:

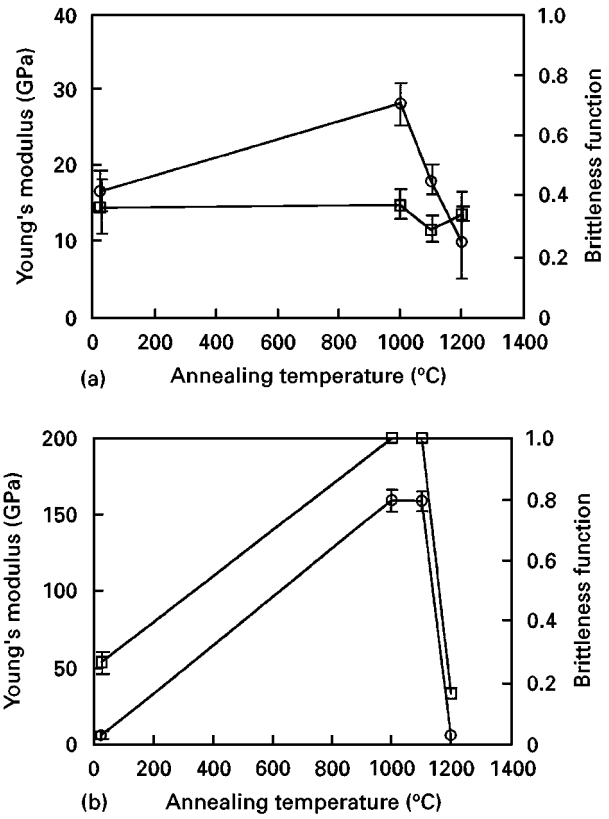

Figure 9 (○) Young's modulus and (□) brittleness function of (a) the Fe–AT and (b) Mg–AT measured at room temperature as a function of the annealing temperature.

1. The two materials showed a unique microstructural feature of extensive microcracking, which led to pronounced inelastic stress–strain behaviour, low strength, Young's modulus, brittleness function and increased crack resistance (R-) curve.

2. The iron-containing material showed no dissociation when annealed for 250 h at 1100 °C, and 1000 h at 1000 and 1200 °C. Therefore, no pronounced changes in mechanical properties were observed after annealing.

3. The magnesium-containing material showed pronounced decomposition into rutile and corundum during long-term annealing in the temperature range 1000–1200 °C, the extent of which is more pronounced at 1000 and 1100 °C. The decomposition product has a finer grain size and is nearly free of microcracking, leading to higher strength and Young's modulus, but also brittle fracture behaviour.

4. At 1000 °C, both materials showed an increase in strength and Young's modulus caused by the crack-healing effect. At 1100 and 1200 °C, the softening of the glassy phase dictates the mechanical properties, leading to gradual decrease of strength and Young's modulus.

Acknowledgements

The authors thank Edward Mehrtens for conducting part of the mechanical testing, Sammy Leung for SEM study and Frank Van Luyt, Keith McKay and Tim Nichols for preparing the specimens.

References

1. H. A. J. THOMAS and R. STEVENS, *Br. Ceram. Trans. J.* **88** (1989) 144.
2. *Idem*, *ibid.* **88** (1989) 184.
3. M. ISHITSUKA, T. SATO, T. ENDO and M. SHIMADA, *J. Amer. Ceram. Soc.* **70** (1987) 69.
4. J. P. DAY and R. J. LOCKER, in "Enviceram 88", (Deutschen Keramischen Gesellschaft, Berlin, 1989) p. 127.
5. J. A. KUSZYK and R. C. BRADT, *J. Amer. Ceram. Soc.* **53** (1973) 420.
6. J. J. CLEVELAND and R. C. BRADT, *ibid.* **61** (1978) 478.
7. Standards Association of Australia, Australian Standard AS 1774.5 -1989, "Methods for Physical Testing of Refractories and Refractory Materials, The Determination of Density, Porosity and Water Absorption by Evacuation Method."
8. A. I. NADAI, "Theory of Flow and Fracture of Solids" (McGraw-Hill, New York, 1963).
9. G. A. GOGOTSI, Y. L. GRUSHEVSKY and K. K. STRELOV, *Ceram. Int.* **4** (1978) 113.
10. T. S. LIU, Y. W. MAI, M. V. SWAIN and G. GRATHWOHL, *J. Mater. Sci.* **29** (1994) 835.
11. G. BAYER, *J. Less-Common Metals* **24** (1971) 129.
12. D. S. PERERA, M. W. A. STEWART, S. MORICCA and R. L. JEFFRIES, *Int. Ceram. Monographs* **1** (1994) 310.
13. E. M. LEVIN, C. R. ROBINS and H. F. MC MURDIE (eds.) "Phase Diagram for Ceramists", (American Ceramics Society, Westerville, OH, 1964) Fig. 712.
14. *Idem*, *ibid.* Fig. 771.
15. G. TILLOCA, *J. Mater. Sci.* **26** (1991) 2809.
16. D. S. PERERA and D. J. CASSIDY, *J. Mater. Sci. Lett.* **16** (1997) 699.
17. S. HORI, M. YOSHIMURA and S. SOMIYA, *Mater. Res. Symp. Proc.* **60** (1986) 87.
18. I. ALECU, R. J. STEAD and D. S. PERERA, *Int. Ceram. Monogr.* **1** (1994) 868.

Received 11 November 1996
and accepted 24 September 1997